

He II EMISSION IN Ly α NEBULAE: AGN OR COOLING RADIATION?¹

C. SCARLATA, J. COLBERT, H. I. TEPLITZ, C. BRIDGE
Spitzer Science Center, 314-6, Pasadena, CA-91125

P. FRANCIS², P. PALUNAS³, B. SIANA⁴, G. M. WILLIGER^{5,6,7} AND B. WOODGATE⁸
Apj, *accepted*

ABSTRACT

We present a study of an extended Ly α nebula located in a known overdensity at $z \sim 2.38$. The data include multiwavelength photometry covering the rest-frame spectral range from 0.1 to 250 μ m, and deep optical spectra of the sources associated with the extended emission. Two galaxies are associated with the Ly α nebula. One of them is a dust enshrouded AGN, while the other is a powerful starburst, forming stars at $\sim 600M_{\odot} \text{ yr}^{-1}$. We detect the He II emission line at 1640 \AA in the spectrum of the obscured AGN, but detect no emission from other highly ionized metals (C IV or N V) as is expected from an AGN. One scenario that simultaneously reproduces the width of the detected emission lines, the lack of C IV emission, and the geometry of the emitting gas, is that the He II and the Ly α emission are the result of cooling gas that is being accreted on the dark matter halo of the two galaxies, Ly1 and Ly2. Given the complexity of the environment associated with our Ly α nebula it is possible that various mechanisms of excitation are at work simultaneously.

Subject headings: high redshift galaxies large scale structure

1. INTRODUCTION

Searches for high redshift Ly α emitters are now successfully finding large samples of normal star-forming galaxies at redshifts up to $z \sim 6$. These searches are also discovering rare, extremely powerful and spatially large Ly α sources, often referred to as “blobs” in the literature (Steidel et al. 2000). Ly α nebulae are characterized by extended Ly α emission on scales up to hundreds of kiloparsecs. The total integrated luminosity in nebulae can exceed $10^{43} \text{ erg s}^{-1}$, that is, more than $10^{10}L_{\odot}$ of energy is emitted in just the Ly α line itself. These nebulae are similar both in energy output and morphology to the emission line nebulae associated with powerful high redshift radio galaxies, however no radio sources have been detected in their proximity. The number density of these sources is still poorly known, mainly because of the rarity of these sources; Yang et al. (2008) find only 4 Ly α nebulae in a survey targeting $z = 2.3$ over an area of $\sim 5 \text{ deg}^2$. The Ly α nebulae were first discovered by Steidel et al. (2000), (see also Francis et al. 1996, 1997), in a region characterized by an overdensity of galaxies by about a factor of 6 when compared to the field population. Since then, most other nebulae have also been discovered in overdense regions of the Universe (Prescott et al. 2008; Matsuda et al. 2004).

Apart from their extended size, what makes Ly α nebulae peculiar compared to normal star forming Ly α emit-

ters is the lack of an obvious source of ionization for the gas. Various mechanisms have been proposed to explain the observed emission, including photoionization by either powerful AGNs or starbursts (with the ionizing radiation escaping toward the nebula, rather than the observer; Steidel et al. 2000), shocks produced by supernova driven winds (Taniguchi & Shioya 2000; Mori et al. 2004), and cooling radiation from gas falling into a dark matter halo (Fardal et al. 2001; Yang et al. 2006).

The latter model is of particular interest in light of recent theoretical studies showing that a substantial fraction of the in-falling gas does not shock heat to the virial temperature of the dark matter halo, but arrives at the central galaxy predominantly along filaments in the cosmic web (Kereš et al. 2005; Dekel & Birnboim 2006; Dekel et al. 2008; Brooks et al. 2008). Such cold streams could be responsible for the observed Ly α nebulae (Yang et al. 2006). This mode of gas accretion is predicted to be the way by which massive galaxies at $z \sim 2$ can still acquire gas that can be turned into stars. However, an observational confirmation of this mechanism is still missing, although a few possible examples have been presented in the past few years (Nilsson et al. 2006; Smith & Jarvis 2007; Smith et al. 2008).

Here we present an in-depth study of a complex Ly α nebula at $z \sim 2.38$ found to be associated with multiple 24 μ m sources (Palunas et al. 2004; Colbert et al. 2006). This Ly α nebula (RA= 21 : 42 : 42.72, DEC= -44 : 30 : 00.0) is located within a large structure of Ly α emitting galaxies, in an $80 \times 80 \times 60$ comoving Mpc region surrounding the known $z = 2.38$ group of galaxies J2143-4423 (Francis et al. 1996). The structure is defined by ~ 30 spectroscopically confirmed Ly α emitters (Francis et al. 2004), a space density a factor of 5.8 ± 2.5 greater than that found by field samples at similar redshifts. The distribution of the Ly α emitters is possibly filamentary, and contains several 5 – 10 Mpc scale voids.

¹ Based in part on observations obtained with the *Spitzer Space Telescope*, which is operated by JPL, California Institute of Technology for the National Aeronautics and Space Administration

² The Australian National University

³ Carnegie Observatories

⁴ Caltech

⁵ University of Louisville

⁶ Johns Hopkins University

⁷ Catholic University

⁸ NASA/ Godard Space Flight Center, USA

This group of galaxies was first discovered as a cluster of Lyman limit absorption-line systems along the line of site of two $z > 3$ QSOs (Francis et al. 2001; Francis & Hewett 1993).

The paper is organized as follows. Section 2 describes the imaging and spectroscopic data, Section 3 present the results. The origin of the galaxies associated with the nebula is studied in Section 4, while in Section 5 we discuss various plausible mechanisms for the gas ionization. Section 6 presents our conclusions. Throughout the paper we assume $\Omega_m = 0.3$, $\Omega_m + \Omega_\Lambda = 1$, and $H_0 = 70$ km s $^{-1}$ Mpc $^{-1}$. All magnitudes are AB magnitudes (Oke 1974), unless otherwise specified.

2. OBSERVATIONS AND DATA ANALYSIS

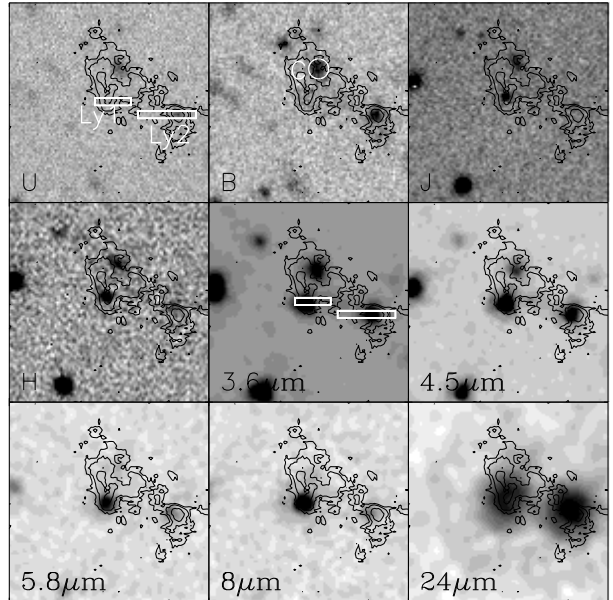
2.1. Imaging data

The J2143–4423 field is a well studied area of the sky, with deep imaging from X-ray to the radio wavelengths (Table 1). This wealth of data allows an in depth study of the Ly α nebula. The optical and NIR data, including *U*, *B*, *G*, *R*, narrow band centered at 4107Å, *J* and *H* images were acquired at the Cerro Tololo Interamerican Observatory (CTIO) 4m telescope, using the Mosaic II imager, and the near Infrared Side Port Imager camera (ISPI). Mid-IR images of the field were taken with the four channels of the Infrared Array Camera (IRAC, Fazio 2004) at 3.6, 4.5, 5.8 and 8.0 μ m and with the Multi-band Imaging Photometer (MIPS, Rieke 2004) at 24 μ m on the *Spitzer* Telescope. The data reduction of the optical and infrared data will be discussed in detail in a companion paper presenting the stellar population properties of all Ly α emitters identified in the cluster field (Scarlata 2010, in preparation). Observations at 850 μ m were obtained with CCAT+LaBoca installed on the Atacama Pathfinder EXperiment and presented in Beelen et al. (2008). X-ray data covering 0.5-10 keV were acquired with Chandra+ACIS (Williger 2010, in preparation). Radio observations at 1334 MHz were acquired with the compact array of the Australian telescope (Francis et al. 1996). No radio sources are detected (apart from the $z = 3$ QSO 2139-4434) in the field, down to a 3σ limit of 3.3 mJy.

In Figure 1 we show cut outs of the multiband optical through MIR images, centered at the position of the Ly α nebula⁹. The stamps are 220 kpc on a side at the redshift of the nebula. The Ly α emission, indicated with the solid contours in Figure 1, covers three continuum sources indicated in the figure as Ly1, Ly2 and C. Multislit spectroscopy obtained with the Inamori Magellan Areal Camera and Spectrograph (IMACS) at the Magellan Baade telescope in August 2008 showed that source C is a foreground galaxy at redshift $z = 0.82$. Hereafter we will only consider the two sources Ly1 and Ly2, that are found to be at the same redshift of the extended Ly α nebula (see below).

The available data allow a detailed description of the spectral energy distribution (SED) of the sources detected within and in the vicinity of the $z = 2.38$ Ly α nebula. Particular care needs to be taken in measuring the multiwavelength SED of the objects due to the intrin-

⁹ For displaying purposes only, we show all images with the same orientation and pixel scale. The photometry measurements were performed on the original exposures.



[t]

FIG. 1.— Images of the area around the Ly α nebula. The images are 27 arcseconds on the side (corresponding to ~ 220 kpc at $z = 2.37$). From top left, to bottom right, we show *U*, *B*, *J*, *H*, IRAC channels 1, 2, 3, 4 and MIPS 24 μ m. The contours in each image show the diffuse Ly α emission, and represent 3, 4, and $5 \times \sigma_{Ly\alpha}$ ($\sigma_{Ly\alpha} = 2 \times 10^{-18}$ erg cm $^{-2}$ s $^{-1}$ arcsec $^{-2}$). The white boxes overlotted to the *U* and 3.6 μ m images show the positions and orientation of the slits. The names of the two $z = 2.38$ galaxies are indicated near the slit. The position of the foreground object, *C*, is also shown.

sically different spatial resolution of the various datasets. Since both Ly1 and Ly2 appear unresolved even in the best quality images available (0'9 full width half maximum, FWHM, in the *J* and *H* images), we computed their total flux within a circular aperture with a diameter optimized independently for each band. The aperture size was chosen to be large enough to include as much flux as possible from the source, while maximizing the signal-to-noise ratio within the aperture and minimizing the contamination by nearby sources. The aperture diameter was typically chosen to be $1.5 \times$ the FWHM. The aperture magnitudes were then transformed into total magnitudes by applying an aperture correction derived for each image using isolated pointlike sources. We also computed Kron-like elliptical aperture total magnitudes using SeXtractor (Bertin & Arnouts 1996), and we verified that the results do not differ from those obtained with circular apertures. The broad band total magnitudes for Ly1 and Ly2 are shown in Table 2.

2.2. Spectroscopic data

Multi object spectroscopy was performed in the region surrounding the Ly α nebula using the Gemini Multi Object Spectrograph (GMOS Hook 2003) on Gemini South. The optical spectroscopy targeted the objects associated with the nebulae, and nearby 24 μ m sources. The spectra were obtained with the B600 grating, tilted at two different angles (corresponding to central wavelengths of 4820 and 4870Å). With this setup we were able to cover the entire spectral range between 3700 and 6000 Å, removing the gap between the two CCDs of the camera. In order

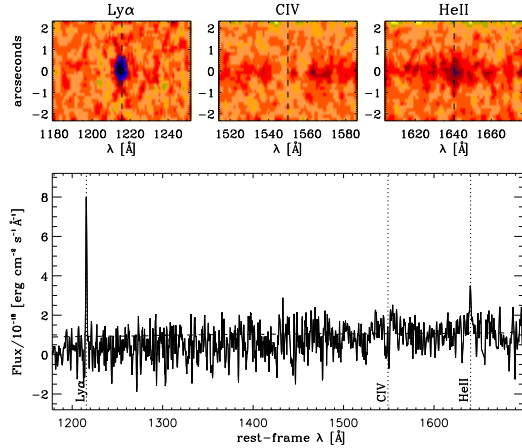


FIG. 2.— GMOS rest frame UV spectrum of Ly1. The extracted spectrum is shown in the bottom panel (solid line), and the 1σ error is shown with a dashed line. The spectrum was smoothed with a boxcar average over 2.7\AA . The dotted vertical lines show the position of the Ly α , C IV, and He II emission lines. In the upper part of the Figure, we show portions of the 2 dimensional spectra centered at the wavelength of the observed emission line features, namely Ly α and He II, and at the expected wavelength of the C IV line.

to increase the signal to noise ratio of the spectra, we binned the images by 2×2 pixels during the read out. The pixel scale of the CCD is $0''.0727 \text{ pixel}^{-1}$ and the seeing conditions were $0''.8$. Thus, the binning does not cause any significant loss in either spatial or wavelength resolution. After binning they are $0''.15 \text{ pixel}^{-1}$ and $0.9 \text{\AA} \text{ pixel}^{-1}$, respectively. The mask was observed for a total of 4.7 hours ($8 \times 2100\text{s}$), with clear conditions and seeing of $0''.8$ FWHM. The slitlets in the mask were $1''$ wide.

The data were reduced using the `gsmos` task included in the IRAF gemini package. Briefly, the reduction steps include bias subtraction, slit by slit flat-field normalization, wavelength calibration, and 2d spectral rectification. Wavelengths were calibrated using the arc line exposures, yielding a solution with an rms error of approximately 0.3\AA . The sky was measured in each slit by fitting a function (either a constant or an order 2 Chebyshev function) to a selected sample of pixels in each column of the slit. One dimensional spectra were extracted with `gsextract` in IRAF¹⁰ (Tody 1993).

The spectral resolution, measured from the emission lines of the lamp spectra, is 5.0\AA (FWHM), corresponding to a velocity resolution of $\sim 310 \text{ km s}^{-1}$ at 4850\AA . We removed the wavelength-dependent instrumental response using the response curve derived from the spectrum of a standard star. The spectra were flux calibrated using the broadband B magnitudes of Ly2 (see Figure 1). We convolved the extracted spectrum with the B -band filter transmission curve to obtain the measured flux density (f_{measured}). The ratio ϵ between f_{measured} and the known B -band flux density provides the flux calibration

¹⁰ IRAF is distributed by the National Optical Astronomy Observatories, which are operated by the Association of Universities for Research in Astronomy, Inc., under cooperative agreement with the National Science Foundation.

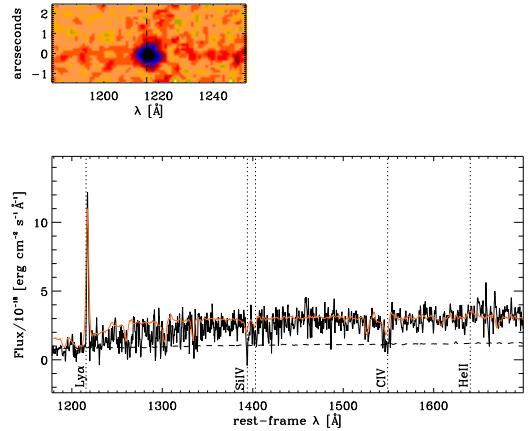


FIG. 3.— Same as Figure 3 for Ly2. The orange spectrum is the composite spectrum derived for $z \sim 3$ LBG by Shapley et al. (2003).

for the spectra ($f_{\lambda,B} = f_{\text{measured}}/\epsilon$). Such a calibration also includes the correction for any flux lost because of the finite size of the slit. Due to the proximity of Ly1 and Ly2, we applied the same calibration factor to both sources. From the error on the broad band magnitude, we estimate a 15% error on the flux calibration.

We obtained mid-infrared spectra for both Ly1 and Ly2 with the *Spitzer* Infrared Spectrograph (IRS), using the 1st order of the Long-Low module (LL1), which is sensitive from $19.5 - 38.0 \mu\text{m}$. The LL1 module has a spatial resolution of $5''.1 \text{ pixel}^{-1}$ and a wavelength resolution of $R = 58 - 116$. The IRS data were acquired on June 13, 2007 (GO-30600, P.I. J. Colbert), using the IRS Spectral Mapping Astronomical Observation Template, placing each source at six separate positions along the length of the slit, separated by $20''$. We used 10 mapping cycles and the 120 second ramp exposure for both, producing a total integration time of 120 minutes for each source. After sky subtraction and correction for latent charge build-up, the data at each position were averaged together and extracted using the *Spitzer* Science Center program SPICE (v.2.1.2) and its optimal extraction option. We then averaged all six spectrum positions together before making a final calibration adjustment based on the known $24 \mu\text{m}$ fluxes. For further data reduction details see Colbert (2009, in preparation).

3. RESULTS

In Figure 1, we can see that the Ly α emission extends over an area of about ~ 100 square arcseconds. It encompasses the two sources of continuum, indicated as Ly1 and Ly2, and shows peaks centered on them. Although the bulk of the extended Ly α emission is localized nearby Ly1, this galaxy is not located at the center of the emission. The total Ly α flux integrated over the entire nebula is $1.5 \times 10^{-15} \text{ erg cm}^{-2} \text{ s}^{-1}$ (Palunas et al. 2004), corresponding to a total luminosity $L_{\text{Ly}\alpha} = 6.5 \times 10^{43} \text{ erg s}^{-1}$ ($1.6 \times 10^{10} L_{\odot}$).

The GMOS slits were positioned over the continuum sources, as indicated by the white boxes in Figure 1. The extracted spectra of Ly1 and Ly2 are shown in Figure 2 and 3, respectively. In the bottom panel of each figure

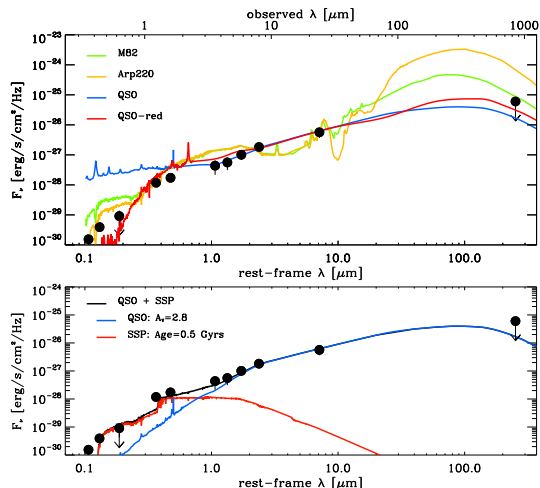


FIG. 4.— Top panel: Spectral energy distribution of Ly1 (circles), compared with template SEDs of different (both active and star-forming) galaxies from the compilation of templates by Polletta (2006). All templates are normalized to the observed $24\mu\text{m}$ flux. Bottom panel: comparison of Ly1 SED (circles) with a composite model (black line) derived by combining a QSO template with an $A_V = 2.8$ magnitudes (blue curve) plus a 0.5 Gyr old stellar population (red curve).

we show the extracted spectrum with the 1σ associated error. In the upper part of the Figure, we show portions of the two dimensional spectra centered at the wavelength of the main features considered in this work, namely $\text{Ly}\alpha$, C IV, and He II $\lambda 1640$ for Ly1 and $\text{Ly}\alpha$ for Ly2. The spectra confirm that both sources are at redshift $z \sim 2.37$, and not a chance superposition with the $\text{Ly}\alpha$ nebula.

Apart from the narrow $\text{Ly}\alpha$ emission line, the spectrum of Ly1 shows an emission line at $\lambda = 5531.7\text{\AA}$, corresponding to He II at redshift $z = 2.373$. No C IV $\lambda 1550$ emission line is detected in the spectrum. To derive an upper limit to the intensity of the C IV emission we added progressively fainter emission lines at the expected wavelength of the line, until it could no longer be identified at the 2σ level. As can be seen in the two dimensional spectrum of Ly1, neither the $\text{Ly}\alpha$ nor the He II emission lines show an extended morphology, and are cospatial with the continuum. The slit, however, was oriented perpendicular to the bulk of the extended emission, so that it covered only the most southern clump (see Figure 1). Not knowing the morphological extension of the He II emission, the total luminosity derived from the observed spectrum can be regarded as a lower limit, since the He II emission could be extended. Estimation of the size of the He II emitting region is limited by the seeing ($\text{FWHM} = 0''.8$) during the observations. The size of the nebula is spatially unresolved so its size is $< \sim 6.5$ kpc.

Ly2 has a bright rest-frame UV continuum, with a B -band (corresponding to $\sim 1300\text{\AA}$ rest-frame) AB magnitude of 23.8, and we are able to identify various absorption lines in its spectrum. The features that we detect come from both low- and high ionization interstellar lines (e.g., Si II 1526, C II 1334, Si IV 1393-1402, C IV 1550), typical of high redshift star-forming galaxies (Shapley et al. 2003). The redshift of Ly2 measured using the absorption lines is $z = 2.362$, slightly lower than the redshift

estimated from the $\text{Ly}\alpha$ emission line ($z_{\text{Ly}\alpha} = 2.367$). Such a difference corresponds to a velocity shift of ~ 450 km s^{-1} , and is in the range of the typical shifts observed in LBGs ($\langle \Delta v \rangle = 650$ km s^{-1} , Shapley et al. 2003). The exact difference, however, is uncertain due to the absorption by the $\text{Ly}\alpha$ forest on the blue side of the line.

The redshifts of the two galaxies place them within the structure of $\text{Ly}\alpha$ emitters. Spectroscopy confirmed the structure to be at a mean redshift of $z = 2.378$, with a standard deviation of 820 km s^{-1} (Francis et al. 2004).

The observed equivalent widths (EWs), velocity dispersion, and line fluxes of the emission lines detected in Ly1 and Ly2 are presented in Table 3. The luminosity of the $\text{Ly}\alpha$ emission measured from both Ly1 and Ly2 accounts for $\sim 10\%$ of the total $\text{Ly}\alpha$ luminosity integrated over the extended nebula. We computed the mean flux density at rest-frame 1500\AA for both Ly1 and Ly2 by averaging the observed flux within a band of $\pm 20\text{\AA}$. Ly1 and Ly2 have $f_{1500} = 8 \pm 5 \times 10^{-19}$ and $2.8 \pm 0.8 \times 10^{-18}$ $\text{erg cm}^{-2} \text{s}^{-1} \text{\AA}^{-1}$, respectively.

4. THE ORIGIN OF THE TWO CONTINUUM SOURCES

The SEDs of the two objects associated with the $\text{Ly}\alpha$ nebula can provide valuable information on the mechanisms responsible for the ionization of the gas. Both sources are characterized by high mid-IR fluxes ($F_{24\mu\text{m}} \sim 0.6 \text{ mJy}$) and are not detected at the submm wavelength. The complete SEDs of Ly1 and Ly2 are shown in Figures 4 and 6. The LaBoca 3σ flux limit of 6 mJy at $850\mu\text{m}$ is also shown.

Ly1: Ly1 is a source of intense emission at $24\mu\text{m}$, corresponding to a $\nu L_\nu \sim 2.3 \times 10^{11} L_\odot$ at rest-frame $\sim 7\mu\text{m}$. The strong mid-infrared flux and its proximity ($9''.5$, corresponding to ~ 80 kpc at $z = 2.38$) to the other powerful $24\mu\text{m}$ source, Ly2, have been suggested to imply that both these galaxies are undergoing a strong burst of star formation, possibly induced by their interaction (e.g., Colbert et al. 2006). Other evidence, however, indicates that Ly1 is a heavily reddened QSO. First, the SED of Ly1 is characterized by a power law shape from 1 to $7\mu\text{m}$ rest-frame, and by a high mid-infrared to optical flux ratio ($f_{24}/f_R \sim 10^3$). These properties, together with the powerful $24\mu\text{m}$ emission of this object, are typical of obscured AGNs as recently suggested by Fiore et al. (2008). In Figure 4, top panel, we compare the SED of Ly1 with templates of active galaxies (taken from Polletta 2007) and local starburst galaxies. All templates are normalized to the $24\mu\text{m}$ observed flux density. Among the Polletta et al. templates, we show the templates of a reddened and of an un-obscured QSO (red and blue curve, respectively). We do not show the templates of the low luminosity Seyfert 2 galaxies, since their SEDs show a pronounced minimum at $\sim 3\mu\text{m}$ that is not consistent with the data of Ly1. We also show Arp220 (yellow curve) and M82 (green curve), since these galaxies have, respectively, the reddest and the bluest $f_{250\mu\text{m}}/f_{7\mu\text{m}}$ rest-frame color.

The shape of the observed SED of Ly1 is clearly inconsistent with Arp220 and M82. At wavelengths shorter than $10\mu\text{m}$ rest-frame, both the M82 and the Arp220 templates are characterized by the $1.6\mu\text{m}$ bump in the SED due to the minimum in the H^- opacity, and by a minimum in the flux density around $3\mu\text{m}$. The minimum at $3\mu\text{m}$ marks the transition between stellar- and dust-

dominated emission. The fact that it is not observed in the Ly1 SED is a strong indication of the presence of a hot dust component, whose emission dominates in the 3 to $5\mu\text{m}$ rest frame, and is usually absent in star-formation dominated galaxies.

The optically selected un-reddened QSO template reproduces well the SED of Ly1 at $\lambda > 1\mu\text{m}$, however it strongly over-predicts its UV energy output. A better agreement to the observed data at short wavelengths is given by the SED of the reddened QSO model, but the UV through optical rest-frame color of this template is too red to match the observed data. The lack of broad emission lines in the optical spectrum of Ly1 indicates that the QSO is heavily obscured, making it likely that the continuum in the optical/UV rest-frame is dominated by the light of the host galaxy (e.g., Urrutia et al. 2008). This is shown in the bottom panel of Figure 4, where we model the SED of Ly1 using a combination of a reddened QSO (blue curve) plus a 0.5 Gyr old stellar population template (red curve). To reproduce the observed SED, the QSO template needs to be reddened by an extinction of $A_V = 2.8$ magnitudes. Assuming the Galactic dust-to-gas ratio ($E(B-V)/N_H = 1.7 \times 10^{-22} \text{ cm}^{-2}$; Maiolino et al. 2001), the column density of Hydrogen would be $\sim 4 \times 10^{21} \text{ cm}^{-2}$. This estimate represents a lower limit, since the dust-to-gas ratio in AGNs is nearly always found to be a factor between 3 and 100 lower than the Galactic one (corresponding to N_H between 1.2×10^{22} and $4 \times 10^{23} \text{ cm}^{-2}$ Maiolino et al. 2001).

Ly1 is not detected in the Chandra images down to a 2σ limit of $f_{0.5-7\text{keV}} = 10^{-15} \text{ erg cm}^{-2} \text{ s}^{-1}$ (corresponding to $L(2-10\text{KeV}) \sim 3 \times 10^{43} \text{ erg s}^{-1}$, assuming a power law spectrum with energy index $\alpha_E = 0.8$, Williger 2010, in preparation). If Ly1 was unabsorbed, its $6\mu\text{m}$ luminosity would imply a rest-frame 2–10 KeV luminosity of a few $10^{44} \text{ erg s}^{-1}$ (Fiore et al. 2008; Lutz et al. 2004), i.e., above the observed Chandra flux limit. To absorb the X-ray luminosity to the observed Chandra limit requires a gas column density of N_H of $\sim 5 \times 10^{22} \text{ cm}^{-2}$, consistent with the range of N_H derived in the previous paragraph.

The *Spitzer* IRS spectrum of Ly1 reveals that the integrated contribution of the polycyclic aromatic hydrocarbons (PAH) emission lines to the total mid-IR flux between 7 and $9\mu\text{m}$ rest-frame is less than 10% (Colbert 2009, in preparation). Strong PAH emission is usually observed in strongly star forming objects, and dominates the MIR spectrum of typical local starbursts.

Although the observed SED of Ly1 is consistent at all wavelengths with that of a reddened QSO, the optical spectrum of Ly1 (see Figure 2) is difficult to explain as a result of photoionization by the QSO continuum. In particular, although the presence of the He II emission is typical of “type 2” QSO spectra, the absence of the C IV emission is puzzling. We will return to this point in Section 5.

Ly2: The rest-frame UV and mid-IR SEDs of Ly2 are shown in Figures 5 and 6. Although extremely powerful at $24\mu\text{m}$ (Ly2 has the same luminosity as Ly1 at $24\mu\text{m}$), the majority of the energy in the mid-IR is due to young-star radiation reprocessed by dust. This is confirmed by both the shape of the rest-frame IR SED, and by the mid-IR spectrum of Ly2, shown in Figure 7. The IR

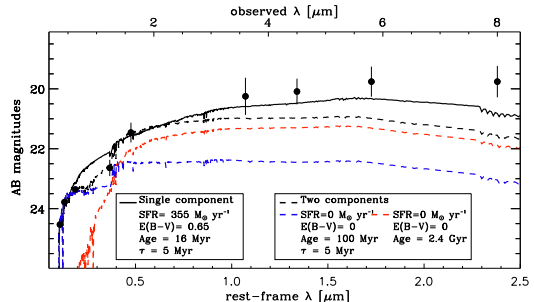


FIG. 5.— Results of the SED fitting to the rest-frame UV to optical photometry of Ly2. The black solid line shows the result of the one component fit, while the dashed line represents the combined spectrum of an old stellar population (red dashed curve) and a young star-forming population (blue dashed curve). The parameters of the two models are indicated in the inset.

SED shows the H^- opacity minimum at $1.6\mu\text{m}$, and the transition to dust dominated emission at about $3\mu\text{m}$. Indeed, the observed $f_{8.0}/f_{4.5}$ color is less than 2, which is typical of $z \sim 2$ star-formation dominated objects (Pope et al. 2008a). The IRS spectrum shows prominent PAH emission lines, whose integrated energy amounts to more than 60% of the mid-IR flux (Colbert 2009, in preparation), confirming the presence of a strong burst of star-formation. In the rest-frame UV, the slope of the continuum measured from the $B-R$ color (i.e., $\sim f_{1900}/f_{1300}$ rest-frame) is rather flat, with $B-R = 0.4 \pm 0.2$ magnitudes. This indicates that the UV is dominated by a young stellar population, with some amount of extinction (Meurer et al. 1999, see Section 4.1). The observed J and H bands bracket the 4000\AA break at the redshift of Ly1. The $J-H$ of 1.1 magnitudes is however too red to be generated by a spectral break alone, and requires substantial dust (see 4.1).

In Figure 6 we compare the mid-IR photometry of Ly2 with three different templates of starburst and normal star-forming galaxies, namely Arp220 (blue curve), M82 (light blue curve), and a late type spiral galaxy (Sc type, yellow curve). As in Figure 4, all templates are normalized to the observed $24\mu\text{m}$ flux density. The $24\mu\text{m}$ flux corresponds to an energy output at $7\mu\text{m}$ rest-frame of $\nu L_\nu > 10^{11} L_\odot$, i.e., for any assumed template SED, Ly2 would be classified as an Ultra Luminous Infrared Galaxy (ULIRG, defined as a galaxy with $L_{IR} > 10^{12} L_\odot$). However, the typical local template for a ULIRG, Arp220, clearly overestimates the flux at $850\mu\text{m}$. The far-to mid-IR flux ratio of Ly2 is more consistent with that of local starburst (such as M82) and normal galaxies (Sc).

In Figure 6 we also show two templates derived by (Pope et al. 2008a) to reproduce the mid-to-far IR SED of dust obscured galaxies at $z \sim 2$ (Desai et al. 2008). These galaxies have typical ULIRG luminosities, however their SED differs from the shape of the local ULIRG template (see also Papovich et al. 2007; Murphy et al. 2008). The total IR luminosity derived using the (Pope et al. 2008a) templates is $L_{IR} = 7 \times 10^{12} L_\odot$. We will use the total IR luminosity in next section to compute the star formation rate (SFR) in Ly2.

4.1. SFR estimate in Ly2

The energetic output of Ly2 is not dominated by emission coming from an active nucleus, but rather from star-formation. The SFR in Ly2 can be measured, or at least constrained, with indicators at different wavelengths. Each of these indicators reflects a different emission mechanism, e.g., direct young star light at 1500\AA rest frame, or cold dust emission at far-IR wavelengths (Kennicutt 1998).

First, we derive the SFR by using the total IR luminosity derived using those templates that satisfy the sub-mm flux limit discussed above. We find consistent values for the estimated IR luminosity of $\sim 3 - 6 \times 10^{12} L_{\odot}$, using both the Sbc and the Pope et al. (2008a) templates. Assuming the Kennicutt (1998) conversion between the IR luminosity and the SFR, we find that Ly2 is forming stars at a rate of $600\text{--}1200 M_{\odot} \text{ yr}^{-1}$.

A second way to estimate the IR luminosity is to use the integrated intensity of the PAH emission lines (e.g. Pope et al. 2008b). The IRS spectrum of Ly2 covers the rest frame wavelength range between 6 and $12 \mu\text{m}$, and the clearest feature detected is the $7.7 \mu\text{m}$ complex. In order to measure the individual PAH emission lines, we used the `PAHfit` software package (Smith et al. 2008). Given the limited coverage of the data, we only include in the fit the lines and one red continuum. The fit to the Ly2 IRS spectrum is shown in Figure 7. We find an integrated luminosity in the $7.7 \mu\text{m}$ complex of $\sim 6.25 \times 10^{10} L_{\odot}$. Using the Pope et al. (2008b) relation between the line luminosity and L_{IR} and the Kennicutt conversion to SFR, we find an SFR of $\sim 1500 M_{\odot} \text{ yr}^{-1}$, consistent with the value inferred from the SED templates. However, this estimate is subject to a large uncertainty. Indeed, Murphy et al. (2008) reanalyzed the Pope et al. (2008b) galaxy sample using a different fitting method, and found L_{IR} a factor of up to ~ 4.8 smaller.

As a third approach to measure the SFR, we perform a complete SED fit to the observed photometric points, including the data between the rest-frame 0.1 to $3 \mu\text{m}$. (The advantage of fitting the full SED rather than using just the UV luminosity is that the former provides the freedom to vary the star formation history and the age of the stellar population). In the fits, we use the Starburst99 stellar population models (Leitherer et al. 1999; Vázquez & Leitherer 2005). We consider a Salpeter Initial Mass Function, and three star formation histories: single burst stellar population, continuous star formation rate, and exponentially declining star formation rate, with two values for the e-folding time $\tau = 150$ and $\tau = 5$ Myr. We let the age of the stellar population vary, considering 60 steps between 1 Myr and 2.5 Gyr, evenly spaced in log space. We consider only models with a metallicity of $0.4Z_{\odot}$, consistent with metallicity measurements of LBGs at similar redshift (Giavalisco 2002). We account for dust extinction using the dust extinction law of Calzetti (1997). We find that the best fit model is provided by a young stellar population with an exponential star formation history (τ of 5 Myr, an age of 16 Myr, and $E(B - V) = 0.65$). The instantaneous SFR is $355 M_{\odot} \text{ yr}^{-1}$. This model requires a substantial amount of dust to reproduce the red rest-frame UV to optical color.

Alternatively, the red colors of the SED of Ly2 could be due to the presence of an old stellar population dominat-

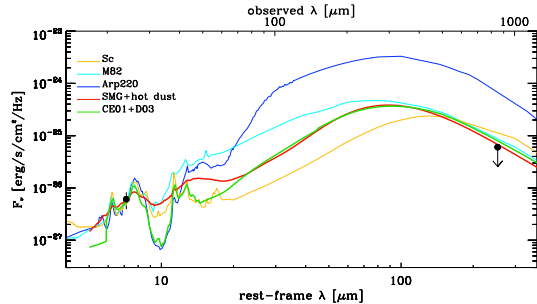


FIG. 6.— Comparison between the IR photometric points of Ly2 at observed $24\mu\text{m}$ and $850\mu\text{m}$ with various starburst templates taken from Polletta (2007) and Pope et al. (2008a).

ing the stellar mass. To check for this, we also perform a two-component fit. The galaxy SED is modeled by the sum of an old stellar population (parametrized with a single burst SED and age of 2.5 Gyr^{11}), and a more recently star-forming population (parametrized with an exponentially declining SFH with $\tau = 5$ Myr). We let the age of the star-forming template vary, and we apply dust extinction only to the star-forming component. In Figure 5, we show the best fit composite SED together with the SEDs of the young and old population, respectively. The age of the young component in the best-fit composite model is of 1.4×10^8 Myr, resulting in a negligible instantaneous SFR. This model can therefore be excluded, since the $24\mu\text{m}$ luminosity and the observed PAH emission clearly indicate that Ly2 is actively forming stars.

To conclude, the analysis of the multi-wavelength data of the two continuum sources associated with the Ly α nebula shows that Ly1 hosts a powerful active nucleus heavily obscured in the rest-frame optical and UV, and whose emission dominates for wavelength $> 1 \mu\text{m}$. Unlike Ly1, the energy output of Ly2 is dominated at all wavelengths by the star-burst. The strength of the burst, quantified with different SFR indicators, ranges from ~ 400 to $\sim 1500 M_{\odot} \text{ yr}^{-1}$.

5. DISCUSSION

The source of energy capable of ionizing the gas in extended Ly α nebulae is still not understood. One of the main reasons for this is that Ly α is a resonant line with a very large cross section, so that various effects, including the geometry of the ISM, the gas velocity field, and the dust absorption, significantly alter the observed Ly α emission, both in its energy output and in the spectral shape of the line. In order to properly model the observed emission, a complete treatment of the radiation transfer of the Ly α photons is needed and this can be done only with simplified assumptions about the dynamical state and chemical composition of the ISM. For these reasons the Ly α emission alone is often not enough to constrain the various mechanisms that have been proposed to explain the source of energy in the Ly α nebulae.

The nebula presented here differs from most other known nebulae, due to the presence of the He II emission line in the spectrum. Unlike the Ly α , He II $\lambda 1640$

¹¹ We note that a difference of ± 1 Gyr in the age of the old stellar population does not change the results.

is not a resonant line and its output is much less affected by the difficulties mentioned above, so that if He II is observed in conjunction with the Ly α , its line width, spatial distribution, and intensity can help establish the source of energy in the emitting gas. The presence of the He II line in the spectrum is a strong constraint for the ionizing source since it requires photons with enough energy to ionize He⁺ (i.e., photons with wavelength $\lambda < 228\text{\AA}$, 54.4 eV).

In this section we will discuss possible mechanisms that can explain the observed emission line spectrum. We will show that the He II emission line is most likely originating from ionized gas located *outside* the Ly1 galaxy, along the line of sight to the observer. Using the limit on the ratio between the C IV and He II emission line intensities as a diagnostic, we also exclude the possibility that the gas is ionized by the continuum of the obscured AGN. Furthermore, we will demonstrate that the possibility that the gas is ionized by a starburst of population III (or very low metallicity) stars is highly unlikely. While not yet proven, the mechanism that simultaneously explains all the observables is cooling radiation from gas falling on the potential well of the dark matter halo of Ly1 and Ly2.

5.1. He II: stellar origin?

As discussed in Section 3, we do not know whether the He II emission is extended (as the Ly α is) or whether it is concentrated on the Ly1 source. We need to consider the possibility that it is of stellar origin, i.e., originating in hot and dense stellar winds of Wolf-Rayet stars. The main observation that argues against this possibility is the width of the He II emission line ($\sigma < 172 \text{ km s}^{-1}$). If the line were created in hot winds its width would be much broader than what is measured in Ly1. In fact, typical WR galaxies have He II emission line widths on the order of thousands of km s^{-1} (Schaerer 2003), while the uncorrected velocity dispersion measured for the Ly1 He II line is $\sigma < 200 \text{ km s}^{-1}$. Furthermore, Leitherer et al. (1995) showed that the emission of He II from hot winds is always associated with a strong P-Cygni emission from C IV $\lambda 1550$, always stronger than He II line emission. As we said in Section 3 we see no C IV emission in the spectrum of Ly1.

5.2. He II: other mechanisms?

The narrow velocity width of the He II line suggests that it is more likely to be of nebular origin. This further suggests that both He II and Ly α originate in gas ionized by a hard continuum source. Only two kinds of sources produce a UV continuum capable of ionizing He⁺: QSOs and extremely metal poor population III stars. As we discussed in Section 4, the two sources of continuum radiation have broad band SEDs consistent with a reddened QSO (Ly1) and a normal star forming galaxy (Ly2). Both are powerful $24\mu\text{m}$ sources and emit a high fraction of their total energy in the mid- and far-IR.

5.2.1. Evidence against an AGN

The continuum of an active nucleus would be hard enough to photoionize He⁺ and produce the observed He II line. We have shown in Section 4 that Ly1 hosts

a heavily obscured active nucleus, so the possibility exists that the emission line spectrum is produced by AGN photoionization. In this section we discuss various pieces of evidence that suggest that the He II and the Ly α emission lines are not the result of photoionization by a QSO continuum, and that the ionized gas is located outside the QSO host galaxy.

The width of the emission lines implies that the broad-line region is completely obscured from our line of sight, and we could be seeing the ionized gas in the intermediate density narrow line region (NLR, $n_H \sim 10^4 - 10^6 \text{ cm}^{-3}$). Typical average values of the line ratios for radio galaxies at $2 < z < 3$ are $\langle \text{Ly}\alpha/\text{HeII} \rangle = 9.80 \pm 5.69$ and $\langle \text{CIV}/\text{HeII} \rangle = 1.50 \pm 0.56$ (McCarthy 1993; Humphrey et al. 2008). Matsuoka et al. (2009) provides the average C IV/He II ratio in bins of He II luminosity and redshift. For $2 < z < 2.5$ and $41.5 < \log(L_{\text{HeII}}) < 42.5$ the average C IV/He II ratio of the NLR is $1.34^{+0.57}_{-0.4}$. In the composite spectrum calculated by (Humphrey et al. 2008) the C IV/He II ratio is 1.75. Therefore the observed line ratios in the spectrum of Ly1 (C IV/He II < 0.8 , Ly α /He II = 2.22 ± 0.98) is inconsistent with the typical high-redshift NLRs at the 90% level. We also note that the typical line width of the He II emission line in HzRGs is of the order of $\geq 500 \text{ km s}^{-1}$ (Humphrey et al. 2008; Villar-Martín et al. 1999).

Shocks could provide an alternative mechanism in cases where large scale outflows and/or radio jets interact with the host galaxy ISM. However, the low C IV/He II ratio can only be produced by shock models when the shock speed exceeds $\sim 400 \text{ km s}^{-1}$, which is inconsistent with the low velocity dispersion measured in the Ly α nebula (Allen et al. 2008).

Matsuoka et al. (2009) recently presented a correlation between the He II luminosity (used as a proxy for the AGN luminosity) and the metallicity of the NLR in high redshift radio galaxies (HzRGs). If produced within the NLR, the observed $L_{\text{HeII}} = 7.9 \times 10^{41} \text{ erg sec}^{-1}$ would imply a gas metallicity of $\sim 0.8Z_{\odot}$, with a large scatter. In their calculations they assume a gas density $n_H = 10^4 \text{ cm}^{-3}$, typical of the intermediate density nuclear NLR (Nagao et al. 2001, 2002). They also find that the measured metallicity of the NLR would not change significantly if the density was two orders of magnitude lower ($n_H = 10^2 \text{ cm}^{-3}$). We can use this metallicity to compare the observed C IV/He II limit with the photoionization models calculated by (Villar-Martín et al. 2007) for the NLR of HzRGs. For metallicity $Z = 0.8Z_{\odot}$ and gas density $n_H = 10^4 \text{ cm}^{-3}$, the Villar-Martín et al. (2007) models predict that C IV/He II ratio should be equal to 1.4 and 2.4, for an ionization parameter¹² U of 0.7 and 0.05, respectively. These ratios are inconsistent with the observed limit. Lower density models ($n_H \leq 10^2 \text{ cm}^{-3}$, typical of low density extended emission line region) predict lower luminosity of the collisionally excited C IV line. However, densities as low as $n_H = 10 \text{ cm}^{-3}$ result in C IV/He II $\geq 0.8 - 1.3$, for $U = 0.7 - 0.05$ Villar-Martín et al. (2007).

If the He II emitting gas is located outside Ly1 it is

¹² $U = Q/4\pi r^2 nc$, where Q is the photo-ionizing luminosity, r is the distance between the gas and the ionizing source, n_H is the total Hydrogen gas density, and c is the speed of light.

most likely associated with the extended Ly α nebula. The He II luminosity implies a rate of He^+ ionizing photons¹³, $Q(He^+)$, of $\sim 1.5 \times 10^{53}$ photons sec^{-1} . As recently suggested by Geach et al. (2009) a fraction of the QSO ionizing continuum could escape the nucleus through an un-obscured direction, and could be enough to power the Ly α nebula. To produce the He II line, the un-reddened continuum should have a rest-frame luminosity at 1350Å of $L_{1350\text{Å}} \sim 4.5 \times 10^{40}$ erg sec^{-1} Å⁻¹, within a factor of two of the measured luminosity of Ly1 at 1350Å. Such a luminosity, however, would still be a factor of at least three too low to account for the total Ly α luminosity in the nebula. In fact, the Ly α luminosity has to be considered as a lower limit, due to the effect of Ly α absorption (e.g, Prescott et al. 2009).

Recently Prescott et al. (2009) presented the discovery of a giant $z = 1.63$ Ly α +He II emission line nebula. They are able to reproduce the observed ratio of C IV/He II= 0.22 with extremely metal poor gas ($Z \leq 10^{-2} - 10^{-3} Z_{\odot}$) ionized by a hard continuum, under certain assumptions for the unconstrained ionization parameter. In our system, however, it is hard to reconcile such a low metallicity gas with the fact that both Ly1 and Ly2 contain significant amount of dust.

From the above discussion we conclude that the gas producing the observed emission line spectrum is most likely not photoionized by the hard continuum of the active nucleus. However, the various parameters entering the photoionization models are largely unconstrained, and more observations are needed to conclusively rule out the AGN interpretation.

5.2.2. Evidence against metal poor stars

Can the radiation produced by stars be responsible for the observed Ly α and He II emission? Schaerer (2003) and Panagia (2003) show that significant nebular He II emission in a cloud photoionized by stars can only be observed in the presence of stars with very low metallicity ($\log(Z/Z_{\odot}) < -5.3$) and/or Population III objects, due to their high effective temperature, and high masses (Tumlinson & Shull 2000; Abel et al. 1998). Normal stellar populations emit hardly any flux below $\lambda = 228\text{Å}$, and so cannot explain the He II emission. Does an exotic population of metal poor stars reside in the starburst galaxy Ly2?

Although it has been suggested that population III stars might be present at redshifts as low as 3 (see, e.g., Jimenez & Haiman 2006), star formation in metal free gas pockets is expected to be very rare and improbable at $z \sim 2.5$ (Scannapieco et al. 2003). More importantly, the large amount of energy emitted by both Ly1 and Ly2 at IR wavelengths, together with the detection of PAH emission, imply very large masses of dust. Therefore, a substantial amount of star formation must have already happened in order to produce it. For the population III scenario to work, the population III starburst must be happening in a pocket of gas unpolluted by metals, while still being attenuated by a screen of dust created in a previous episode of star formation. This combination seems too contrived to be plausible, especially in light of numerical simulations showing that gas mixing is very efficient

within a galaxy after the first episodes of star formation (Tornatore et al. 2007). It is further instructive to examine how much star formation would be required in such a pocket of population III stars.

To first approximation, the nebular emission lines are proportional to the ionizing photon flux escaping the galaxy and (under some assumptions about the IMF, metallicity, and age of the burst) to the SFR of the galaxy (Schaerer 2003). The number of He^+ ionizing photons, $Q(He^+)$, is a strong function of the metallicity of the stellar population, so we consider here only the extreme case of a pure population III starburst. For an escape fraction of 10% ($f_{esc} = 0.1$, Iwata et al. 2008), and neglecting the effect of dust for the present, we find that the minimum star formation rate required to power the Ly α nebula is of $\sim 50 M_{\odot} yr^{-1}$. Since we neglected the dust absorption, this estimate represents a lower limit to the true expected SFR in population III stars. Given the arguments given above, population III stars are unrealistic, and we rule out the presence of metal poor stars as a source of He^+ ionizing flux.

Finally, large-scale outflows driven by a strong starburst in a forming galaxy were proposed as another viable mechanism to explain the Ly α nebulae (Taniguchi & Shioya 2000). Recent high resolution hydrodynamic simulations show that multiple SN explosions in starbursts of a few hundred of $M_{\odot} yr^{-1}$ could result in large scale intense Ly α emission, comparable with the observed one in Ly α nebulae (Mori et al. 2004). However, in these models the configuration of the system is rather symmetrical, with the star forming region located at the center of the ionized gas. From Figure 1 one can see that the starburst galaxy (Ly2) is located at the edge of the main Ly α emitting region.

5.2.3. Cooling radiation?

Another possibility, consistent with the observations, is that the extended Ly α emission is coming from gas losing gravitational energy while falling on a galaxy-size dark matter halo. Fardal et al. (2001) and Kereš et al. (2005) cosmological simulations show that the majority of such infalling gas never reaches the virial temperatures expected for the dark matter halo mass, $\sim 10^6$ K (which would emit primarily in the X-ray), but rather cools to lower temperatures of a few 10^5 K. At these temperatures, both Ly α and He II emission are expected. Although the Ly α is expected to be the strongest line, problems related to the radiative transfer of the Ly α photons, the details of the velocity field of the IGM, and the self shielding of the gas at high densities, make the Ly α predictions very uncertain in these models. A distinctive feature of the cooling radiation is that He lines should be observed, with the He II emission coming mostly from collisionally excited He^+ (Yang et al. 2006). We note however that these models assume primordial compositions for the gas. The presence of metals has an impact on the gas cooling function possibly affecting the predicted intensity of the He II emission line. In the Yang et al. (2006) models the He II line is expected to have velocity widths not larger than $\sigma \sim 300 km s^{-1}$, and a distribution clumpier than that of the Ly α emission. For these reasons, even if the He II emission is expected to be several factors fainter than the Ly α , it can still be de-

¹³ $L_{He II} = 5.67 \times 10^{-12} Q(He^+)$, (Schaerer 2003)

tected with observations similar to those presented here.

Using the Ly α luminosity, we can estimate the mass deposition rate (\dot{M}) due to the cooling gas. The Ly α luminosity of $\sim 6 \times 10^{43}$ erg s $^{-1}$ implies $\sim 10^{61}$ recombinations per year, or $\dot{M} \sim 10^4/n M_{\odot}$ yr $^{-1}$, where n is the number of recombinations per H atom. By considering n in the range between 10–100 (Heckman et al. 1989) we find a mass deposition rate in the range between $\sim 10^2 - 10^3 M_{\odot}$ yr $^{-1}$. The cooling material would then be enough to fuel both the QSO activity and the high star formation rate observed in Ly2.

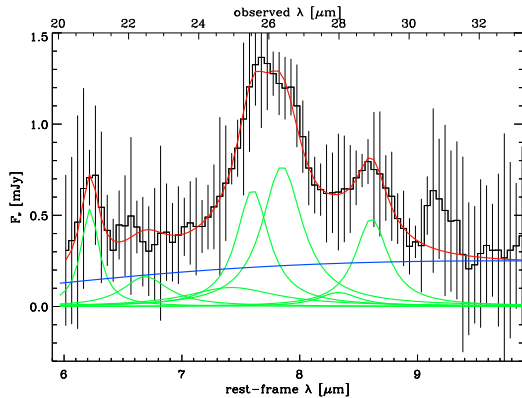


FIG. 7.— IRS spectrum of Ly2 shown as a function of rest-frame wavelength (black curve). The red curve shows the best fit model to the observed spectrum derived combining the PAH emission lines in the rest-frame 6 to $10\mu\text{m}$ (green curves) plus one power law continuum (blue curve).

6. CONCLUSIONS

We have presented a multi-wavelength study of an extended Ly α nebula identified in an over-dense filamentary structure at redshift $z = 2.38$ (Palunas et al. 2004). Two sources (Ly1 and Ly2) of continuum are found to be physically associated with the extended Ly α emission. Both are powerful sources detected at $24\mu\text{m}$, but not detected at either $850\mu\text{m}$ or radio wavelengths, nor in the X-ray. The power-law IR SED of Ly1 is consistent with that of a heavily reddened QSO, while Ly2 is a starburst galaxy, with properties similar to other powerful star-forming galaxies at $z \sim 3$. The UV rest-frame spectra of these two objects confirm that the two galaxies belong to the $z = 2.38$ structure. They have only a small difference in velocity (a few hundred km s $^{-1}$), so it is possible that we are witnessing an early stage of a merger between two massive galaxies.

The rest-frame UV spectrum observed at the position of Ly1 shows emission from He II at 1640 \AA , while we find no associated C IV or N V lines. Although it is possible that the observed emission line spectrum is generated in gas ionized by the continuum of the QSO, the the

observed C IV/He II limit suggests that the Ly α and the He II radiation are the result of a different mechanism. The He II line width argues against a WR stellar origin of the emission line. Extremely metal poor stars can be excluded as a source of ionization because of the presence of metal absorption lines in the UV spectrum of Ly2, and by the presence of dust inferred from the detection of both sources at $24\mu\text{m}$ and the strong PAH lines in Ly2.

Another possibility that would be able to explain the observations is that the He II and the Ly α emission are produced by collisions in gas that is being accreted on the dark matter halo of the two galaxies, Ly1 and Ly2. Future rest-frame optical spectroscopy will help in the interpretation of the Ly α cloud. If due to cold accretion, then the Ly α is caused by collisional excitation rather than photoionization. In this case, the H α line should be only about 2% of the Ly α line (Fardal et al. 2001). Furthermore, the ratio between strong optical ([OIII], H β , H α , and [N II]) emission lines could be used to investigate the source of ionization in the nebula.

Given the complexity of the environment associated with our Ly α nebula it is possible that the various mechanisms of excitation are at work simultaneously. This possibility has been discussed recently by Dijkstra & Loeb (2009), who point out that the association of cold accretion with powerful starburst and/or AGN has to be expected, since ultimately these sources are triggered and fed by the gas infall.

Although theoretically the cold mode of accretion is expected to be the dominant mechanism for growth in massive galaxies at $z \sim 2$ (Dekel et al. 2008), we still lack a direct observational confirmation of its existence. A common prediction among the different models of cold accretion is the unique filamentary morphology expected for the emitting gas. The typical filaments are predicted to have a surface brightness of about $10^{-19.5}$ erg s $^{-1}$ cm $^{-2}$ arcsec $^{-2}$ in both Ly α and He II, and the cooling luminosity is expected to peak at redshifts between ~ 1 and 2. At these redshifts, the Ly α line is barely accessible from the ground and current space based facilities are not sensitive enough to reach the low surface brightness levels in reasonable exposure times. (Reaching a surface brightness of 10^{-19} erg s $^{-1}$ cm $^{-2}$ arcsec $^{-2}$ in the observed Ly α line at $z = 1.8$ with the Hubble Space Telescope Wide Field Camera 3 UVIS channel would require $\sim 10^7$ s). The proposed Advanced Technology Large-Aperture Space Telescope (ATLAS) could potentially detect cooling radiation in the redshift range (between $z = 1$ and 2) where cold flows are expected to be the dominant mechanism for gas accretion in galaxies.

We thank the referee for useful suggestions that improved the discussion of the results. We thank A. Pope for providing the templates in electronic form. C.S. thanks M. Hayes for useful discussions.

REFERENCES

- Abel, T., Anninos, P., Norman, M. L., & Zhang, Y. 1998, *ApJ*, 508, 518
 Allen, M. G., Groves, B. A., Dopita, M. A., Sutherland, R. S., & Kewley, L. J. 2008, *ApJS*, 178, 20
 Beelen, A., Omont, A., Bavouzet, N., Kovács, A., Lagache, G., De Breuck, C., Weiss, A., Menten, K. M., Colbert, J. W., Dole, H., Siringo, G., & Kreysa, E. 2008, *A&A*, 485, 645
 Bertin, E. & Arnouts, S. 1996, *A&AS*, 117, 393

- Brooks, A. M., Governato, F., Quinn, T., Brook, C. B., & Wadsley, J. 2008, ArXiv e-prints
- Calzetti, D. 1997, AJ, 113, 162
- Colbert, J. W., Teplitz, H., Francis, P., Palunas, P., Williger, G. M., & Woodgate, B. 2006, ApJ, 637, L89
- Colbert, J. W. *et al.* 2009, in prep.
- Dekel, A. & Birnboim, Y. 2006, MNRAS, 368, 2
- Dekel, A., Birnboim, Y., Engel, G., Freundlich, J., Goerdt, T., Mumcuoglu, M., Neistein, E., Pichon, C., Teyssier, R., & Zinger, E. 2008, ArXiv e-prints
- Desai, V., Soifer, B. T., Dey, A., Jannuzi, B. T., Le Floch, E., Bian, C., Brand, K., Brown, M. J. I., Armus, L., Weedman, D. W., Cool, R., Stern, D., & Brodwin, M. 2008, ApJ, 679, 1204
- Dijkstra, M. & Loeb, A. 2009, ArXiv e-prints
- Fardal, M. A., Katz, N., Gardner, J. P., Hernquist, L., Weinberg, D. H., & Davé, R. 2001, ApJ, 562, 605
- Fazio, G. G. *et al.* 2004, ApJS, 154, 10
- Fiore, F., Grazian, A., Santini, P., Puccetti, S., Brusa, M., Feruglio, C., Fontana, A., Giallongo, E., Comastri, A., Gruppioni, C., Pozzi, F., Zamorani, G., & Vignali, C. 2008, ApJ, 672, 94
- Francis, P. J. & Hewett, P. C. 1993, AJ, 105, 1633
- Francis, P. J., Palunas, P., Teplitz, H. I., Williger, G. M., & Woodgate, B. E. 2004, ApJ, 614, 75
- Francis, P. J., Williger, G. M., Collins, N. R., Palunas, P., Malumuth, E. M., Woodgate, B. E., Teplitz, H. I., Smette, A., Sutherland, R. S., Danks, A. C., Hill, R. S., Lindler, D., Kimble, R. A., Heap, S. R., & Hutchings, J. B. 2001, ApJ, 554, 1001
- Francis, P. J., Woodgate, B. E., & Danks, A. C. 1997, ApJ, 482, L25+
- Francis, P. J., Woodgate, B. E., Warren, S. J., Moller, P., Mazzolini, M., Bunker, A. J., Lowenthal, J. D., Williams, T. B., Minezaki, T., Kobayashi, Y., & Yoshii, Y. 1996, ApJ, 457, 490
- Geach, J. E., Alexander, D. M., Lehmer, B. D., Smail, I., Matsuda, Y., Chapman, S. C., Scharf, C. A., Ivison, R. J., Volonteri, M., Yamada, T., Blain, A. W., Bower, R. G., Bauer, F. E., & Basu-Zych, A. 2009, ApJ, 700, 1
- Giavalisco, M. 2002, ARA&A, 40, 579
- Heckman, T. M., Baum, S. A., van Breugel, W. J. M., & McCarthy, P. 1989, ApJ, 338, 48
- Hook, I. *et al.* 2003, in Society of Photo-Optical Instrumentation Engineers (SPIE) Conference Series, Vol. 4841, Society of Photo-Optical Instrumentation Engineers (SPIE) Conference Series, ed. M. Iye & A. F. M. Moorwood, 1645–1656
- Humphrey, A., Villar-Martín, M., Vernet, J., Fosbury, R., di Serego Alighieri, S., & Binette, L. 2008, MNRAS, 383, 11
- Iwata, I., Inoue, A. K., Matsuda, Y., Furusawa, H., Hayashino, T., Kousai, K., Akiyama, M., Yamada, T., Burgarella, D., & Deharveng, J. . 2008, ArXiv e-prints
- Jimenez, R. & Haiman, Z. 2006, Nature, 440, 501
- Kennicutt, R. C. 1998, ARA&A, 36, 189
- Kereš, D., Katz, N., Weinberg, D. H., & Davé, R. 2005, MNRAS, 363, 2
- Leitherer, C., Ferguson, H. C., Heckman, T. M., & Lowenthal, J. D. 1995, ApJ, 454, L19+
- Leitherer, C., Schaerer, D., Goldader, J. D., Delgado, R. M. G., Robert, C., Kune, D. F., de Mello, D. F., Devost, D., & Heckman, T. M. 1999, ApJS, 123, 3
- Lutz, D., Maiolino, R., Spoon, H. W. W., & Moorwood, A. F. M. 2004, A&A, 418, 465
- Maiolino, R., Marconi, A., Salvati, M., Risaliti, G., Severgnini, P., Oliva, E., La Franca, F., & Vanzli, L. 2001, A&A, 365, 28
- Matsuda, Y., Yamada, T., Hayashino, T., Tamura, H., Yamauchi, R., Ajiki, M., Fujita, S. S., Murayama, T., Nagao, T., Ohta, K., Okamura, S., Ouchi, M., Shimasaku, K., Shioya, Y., & Taniguchi, Y. 2004, AJ, 128, 569
- Matsuoka, K., Nagao, T., Maiolino, R., Marconi, A., & Taniguchi, Y. 2009, ArXiv e-prints
- McCarthy, P. J. 1993, ARA&A, 31, 639
- Meurer, G. R., Heckman, T. M., & Calzetti, D. 1999, ApJ, 521, 64
- Mori, M., Umemura, M., & Ferrara, A. 2004, ApJ, 613, L97
- Murphy, E. J., Chary, R. R., Alexander, D. M., Dickinson, M., Magnelli, B., Morrison, G., Pope, A., & Teplitz, H. I. 2008, ArXiv e-prints
- Nagao, T., Murayama, T., Shioya, Y., & Taniguchi, Y. 2002, ApJ, 567, 73
- Nagao, T., Murayama, T., & Taniguchi, Y. 2001, ApJ, 546, 744
- Nilsson, K. K., Fynbo, J. P. U., Møller, P., Sommer-Larsen, J., & Ledoux, C. 2006, A&A, 452, L23
- Oke, J. B. 1974, ApJS, 27, 21
- Palunas, P., Teplitz, H. I., Francis, P. J., Williger, G. M., & Woodgate, B. E. 2004, ApJ, 361, L25
- Panagia, N. 2003, Chinese Journal of Astronomy and Astrophysics Supplement, 3, 115
- Papovich, C., Rudnick, G., Le Floch, E., van Dokkum, P. G., Rieke, G. H., Taylor, E. N., Armus, L., Gawiser, E., Huang, J., Marcellac, D., & Franx, M. 2007, ApJ, 668, 45
- Polletta, M. d. C. *et al.* 2006, ApJ, 642, 673
- Polletta, M. *et al.* 2007, ApJ, 663, 81
- Pope, A., Bussmann, R. S., Dey, A., Meger, N., Alexander, D. M., Brodwin, M., Chary, R.-R., Dickinson, M. E., Frayer, D. T., Greve, T. R., Huynh, M., Lin, L., Morrison, G., Scott, D., & Yan, C.-H. 2008a, ApJ, 689, 127
- Pope, A., Chary, R.-R., Alexander, D. M., Armus, L., Dickinson, M., Elbaz, D., Frayer, D., Scott, D., & Teplitz, H. 2008b, ApJ, 675, 1171
- Prescott, M. K. M., Dey, A., & Jannuzi, B. T. 2009, ArXiv e-prints
- Prescott, M. K. M., Kashikawa, N., Dey, A., & Matsuda, Y. 2008, ApJ, 678, L77
- Rieke, G. H. *et al.* 2004, ApJS, 154, 25
- Scannapieco, E., Schneider, R., & Ferrara, A. 2003, ApJ, 589, 35
- Scarlata, C. *et al.* 2010, in prep.
- Schaerer, D. 2003, A&A, 397, 527
- Shapley, A. E., Steidel, C. C., Pettini, M., & Adelberger, K. L. 2003, ApJ, 588, 65
- Smith, D. J. B. & Jarvis, M. J. 2007, MNRAS, 378, L49
- Smith, D. J. B., Jarvis, M. J., Lacy, M., & Martínez-Sansigre, A. 2008, MNRAS, 389, 799
- Steidel, C. C., Adelberger, K. L., Shapley, A. E., Pettini, M., Dickinson, M., & Giavalisco, M. 2000, ApJ, 532, 170
- Taniguchi, Y. & Shioya, Y. 2000, ApJ, 532, L13
- Tody, D. 1993, in Astronomical Society of the Pacific Conference Series, Vol. 52, Astronomical Data Analysis Software and Systems II, ed. R. J. Hanisch, R. J. V. Brissenden, & J. Barnes, 173–+
- Tornatore, L., Ferrara, A., & Schneider, R. 2007, MNRAS, 382, 945
- Tumlinson, J. & Shull, J. M. 2000, ApJ, 528, L65
- Urrutia, T., Lacy, M., & Becker, R. H. 2008, ApJ, 674, 80
- Vázquez, G. A. & Leitherer, C. 2005, ApJ, 621, 695
- Villar-Martín, M., Fosbury, R. A. E., Binette, L., Tadhunter, C. N., & Rocca-Volmerange, B. 1999, A&A, 351, 47
- Villar-Martín, M., Humphrey, A., De Breuck, C., Fosbury, R., Binette, L., & Vernet, J. 2007, MNRAS, 375, 1299
- Williger, G. M. *et al.* 2010, in prep.
- Yang, Y., Zabludoff, A., Tremonti, C., Eisenstein, D., & Davé, R. 2008, ArXiv e-prints
- Yang, Y., Zabludoff, A. I., Davé, R., Eisenstein, D. J., Pinto, P. A., Katz, N., Weinberg, D. H., & Barton, E. J. 2006, ApJ, 640, 539

TABLE 1
OPTICAL IMAGE QUALITY AND FLUX LIMITS.

Band	FWHM ^(a) ["]	5σ	Reference
<i>U</i>	1.1	26.0 ^(b)	Scarlata (2010, in preparation)
<i>B</i>	1.4	26.2	Palunas et al. (2004)
<i>R</i>	1.3	24.0	Scarlata (2010, in preparation)
<i>J</i>	0.9	22.9	Scarlata (2010, in preparation)
<i>H</i>	0.9	22.7	
3.6 μ m	1.7	24.3	Colbert (2009, in preparation)
4.5 μ m	1.7	23.5	
5.8 μ m	1.9	21.4	
8.0 μ m	1.9	21.2	
24 μ m	5.4	19.4	Colbert et al. (2006)
870 μ m		8 ^(c)	Beelen et al. (2008)

^(a)In the optical and near-IR images the magnitude limits were computed within an aperture of $1.5 \times \text{FWHM}$ diameter.

^(b)In AB magnitudes.

^(c)In mJy.

TABLE 2
BROAD BAND PHOTOMETRY (AB MAGNITUDES).

Objects	<i>U</i>	<i>B</i>	<i>R</i>	<i>J</i>	<i>H</i>	3.6 μ m	4.5 μ m	5.8 μ m	8.0 μ m	24 μ m
Ly1	25.9 \pm 0.3	24.9 \pm 0.1	> 24.5	21.2 \pm 0.1	20.8 \pm 0.1	19.8 \pm 0.5	19.5 \pm 0.4	18.9 \pm 0.3	18.2 \pm 0.3	17.0 \pm 0.3
Ly2	24.5 \pm 0.1	23.8 \pm 0.1	23.4 \pm 0.2	22.6 \pm 0.3	21.5 \pm 0.1	20.2 \pm 0.6	20.1 \pm 0.4	19.8 \pm 0.5	19.8 \pm 0.5	16.9 \pm 0.3

TABLE 3
EMISSION LINE PROPERTIES.

	Flux erg cm ⁻² s ⁻¹	<i>EW</i> Å	<i>FWHM</i> ^(a) km s ⁻¹
Ly1	$z = 2.373$		
Ly α	$5.0 \pm 0.7 \times 10^{-17}$	131.2 \pm 25.9	< 366
He II	$1.8 \pm 0.7 \times 10^{-17}$	14.2 \pm 4.1	< 400
C IV	$< 1.5 \times 10^{-17}$ ^(b)	–	–
Ly2	$z = 2.367$		
Ly α	$7.3 \pm 0.7 \times 10^{-17}$	67.3 \pm 19.7	202

^(a)The FWHM is not corrected for instrumental resolution.

^(b) 2σ limit, see text for details.